Kinetic investigations of nonlinear electrostatic excitations in quantum plasmas

Tian-Xing Hu, Jiong-Hang Liang, and Zheng-Mao Sheng*
Institute for Fusion Theory and Simulation, School of Physics, Zhejiang University, Hangzhou 310027, China

Dong Wu†
Key Laboratory for Laser Plasmas and School of Physics and Astronomy, Collaborative Innovation Center of IFSA, Shanghai Jiao Tong University, Shanghai 200240, China.

For plasmas in extremely high-density state, like stellar cores or compressed fuel in the inertial fusion facilities, their behavior turns out to be quite different when compared with those plasmas in the interstellar space or magnetic confinement devises. In order to figure out such differences and uncover the kinetic physics in electrostatic excitations, a quantum kinetic code solving Wigner-Possion equations has been developed. Basic plasmon decay, Landau damping and two stream instability of extremely high density plasmas are investigated by using our newly developed code. Numerical simulations show that in the linear region, the dispersion relations of intrinsic modes can be significantly affected by quantum effects, and such simulation results can be well described by the existing analytical theory. Especially in the nonlinear region, since the space-time scale of collective modes of plasmas are comparable to electron de Broglie wavelength, their couplings produce some new physics: the energy exchange between the electron and collective mode result in an abnormal oscillation which does not exist in classical plasmas.

I. INTRODUCTION

When a plasma is dense enough such that the average distance among electrons is comparable to or even smaller than their thermal de Broglie wavelength, the plasma then enters into quantum regime [1]. Quantum plasmas are also widely exiting in the universe. The study of quantum plasma is of great significance in many different fields of physics, such as inertial confinement fusion (ICF) [2], nano-physics [3], astrophysical plasmas [4, 5] and warm dense matter (WDM) [6]. Quantum plasma differs from regular plasma in the following two aspects: 1) the equilibrium state of quantum plasma obeys the Fermi-Dirac statistics instead of the Maxwellian because of the overlapping of electron spacial wave function; 2) the quantum wave effect of single electron alters the collective behavior of quantum plasma since they (the quantum wave and the plasma wave) have a comparable space-time scale.

The state-of-the-art approaches for investigating quantum plasmas are those based on the density-functional theory (DFT) [7, 8]. The DFT-based methods are often combined with the molecular dynamics (MD) method or quantum Monte Carlo (QMC) method [9–11], in order to achieve desirable accuracy in a variety of parameter regions. However, the DFT-based methods usually focus on the microscopic structure of matters, for example, the lattice of solids or the shape of molecules, and only involve a small number of particles (ranging from hundreds to thousands). Hence, it is not suitable for macroscopic or mesoscopic systems in which the number of particles is almost uncountable.

In order to investigate a macroscopic or mesoscopic system, a statistical method is often needed. The most popular simulation method in plasma physics community is kinetic method. In classical plasmas, Vlasov equation is often used, with the distribution function determined by spatial position and velocity. However, in quantum mechanics, the coordinate and the velocity of a particle cannot be determined simultaneously due to the uncertainty principle. Hence, a particle with a definite phase space coordinate is ill-defined in a quantum mechanical system. Nevertheless, the quantum kinetic method with Wigner's quasi-distribution function [12] and the Wigner equation [13] bring us a mean to bypass this obstacle.

The quantum kinetic theory (QKT) starts from second-quantized many-body quantum theory, which convert the equation of motion of the quantum field operator into a Boltzmann-like transport equation, with interactions beyond the Hartree mean-field approximation included in the collisional term [13–15]. Hence, QKT is of great potential in calculating high-order quantum correlations[16]. Analog to the fluid description in classical plasma [17], the quantum hydrodynamics (QHD) treats the quantum electron gas as a fluid [17]. The equation of motions of the quantum fluid can be simplified into a single nonlinear Schrödinger equation. Although the QHD is less cumbersome and in the last two decades, a lot of work has been done by using QHD [18–21], its accuracy is yet to be tested [22, 23].

In this paper, we take the collisionless quantum kinetic equation, i.e., the Wigner equation [13] as a starting point to investigate the quantum nature of dense plasma. The ions are assumed to be static and serve as a neutralization background throughout this paper. A modified numerical method is adopted. Theory and numerical simulations show that even in the linear region, the dispersion relations of intrinsic modes can be significantly affected by quantum effects. Especially in the nonlinear region,

* zmsheng@zju.edu.cn
† dwu.phys@sjtu.edu.cn

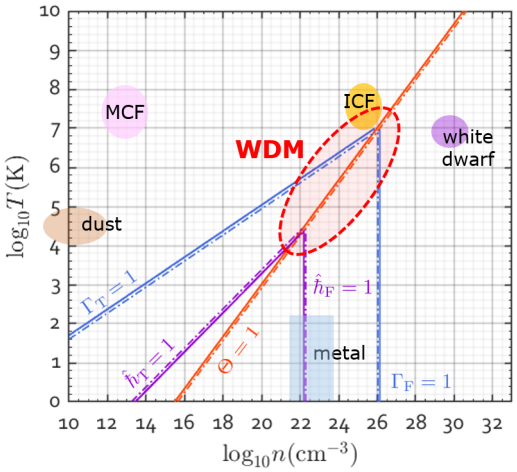

Figure 1. Relation among different characteristic parameters of quantum plasmas. The solid line represent the region with the corresponding parameter greater than one, while the dashed-line the opposite [6].

since the space-time scale of collective modes of plasmas are comparable to electron de Broglie wavelength, their couplings produce some new physics. For example, a single-particle-quantum-oscillator-like structure is found in a quantum BGK equilibrium. Further more, energy exchange between the electron and collective mode result in an abnormal oscillation which does not exist in classical plasmas.

This paper is organized as follows. In section II, we briefly review the basic ideas of QKT, and then our numerical method is brief introduced. Section III displays the basic plasmon decay and quantum Landau damping in the linear region. And in section IV, the nonlinear evolution of a quantum two-stream instability is studied in detail.

II. METHODS

A. Description of Quantum Plasmas

Firstly, it is natural to define a general normalized Planck constant (NPC):

$$\hat{\hbar}_{\mathrm{c}}=\frac{\hbar\omega_{\mathrm{p}}}{mv_{\mathrm{c}}^2}, \tag{1}$$

where m is the mass of electron, and v_{c} stands for a critical velocity of the physical system. For example, if we choose Fermi or thermal velocity as the critical velocity, we have

$$\hat{\hbar}_{\mathrm{F}}=\frac{\hbar\omega_{\mathrm{p}}}{2\mathcal{E}_{\mathrm{F}}},\quad \hat{\hbar}_{\mathrm{T}}=\frac{\hbar\omega_{\mathrm{p}}}{2k_{\mathrm{B}}T}, \tag{2}$$

respectively. Here, $k_{\mathrm{B}}T$ is the thermal energy of electrons, $\omega_{\mathrm{p}}=\sqrt{4\pi ne^2/m}$ is the plasma frequency, and the Fermi energy $\mathcal{E}_{\mathrm{F}}=\hbar^2\left(3\pi^2n\right)^{2/3}/2m_e$ is the chemical potential of a degenerate zero-temperature electron gas. Noticing that these two NPCs are related by the degeneracy of the system:

$$\Theta=\frac{\hat{\hbar}_{\mathrm{F}}}{\hat{\hbar}_{\mathrm{T}}}=\frac{k_{\mathrm{B}}T}{\mathcal{E}_{\mathrm{F}}}, \tag{3}$$

and, $\hat{\hbar}_{\mathrm{F}}$ is only the function of density:

$$\hat{\hbar}_{\mathrm{F}}=5.09\times10^3\mathrm{cm}^{-\frac{1}{2}}n^{-\frac{1}{6}}, \tag{4}$$

and $\hat{\hbar}_{\mathrm{T}}$ is suitable for situations in which the temperature is high enough to disguise the Fermi statistic effect while the quantum effect still exists to some extent. Another famous pair of characteristic parameters is

$$\Gamma_{\mathrm{F}}=\frac{e^2n^{\frac{1}{3}}}{\mathcal{E}_{\mathrm{F}}},\quad \Gamma_{\mathrm{T}}=\frac{e^2n^{\frac{1}{3}}}{k_{\mathrm{B}}T}. \tag{5}$$

They are the ratio between Coulomb potential energy and Fermi/Thermal energy. The traces of characteristic parameters mentioned above equal to one respectively are plotted in Fig. 1, from which one can see that $\Theta=\hat{\hbar}_{\mathrm{F}}=\hat{\hbar}_{\mathrm{T}}=1$ stands for a low-density-low-temperature WDM, and $\Theta=\Gamma_{\mathrm{F}}=\Gamma_{\mathrm{T}}=1$ a high-density-high-temperature WDM.

The velocity distribution obeys the Fermi-Dirac statistics:

$$f_{\mathrm{FD3}}(v)=\frac{3n}{4\pi}\frac{1}{\mathrm{e}^{(v^2-\hat{\mu})/\Theta}+1}, \tag{6}$$

where $\hat{\mu}(\Theta)=\mu(T)/\mu(0)$ is the chemical potential normalized by Fermi energy. Furthermore, when we are discussing wave-particle interactions, only one direction of the velocity, namely, the direction that is parallel to the wave, has to be considered. Hence, we can remove the extra two dimensions by integration and then obtain the one-dimensional Fermi-Dirac distribution

$$f_{\mathrm{FD1}}(v_\parallel)=\frac{3n}{4}\Theta\ln\left[\mathrm{e}^{(\hat{\mu}-v_\parallel^2)/\Theta}+1\right]. \tag{7}$$

An important difference between the quantum and the classical kinetic theory is that the distribution function of the former can take on negative values. This is because in QKT, the distribution function is defined by [13]

$$\begin{aligned} f(\boldsymbol{x},\boldsymbol{v})=&\frac{1}{(2\pi\hbar)^3}\int \mathrm{d}\boldsymbol{\xi}\mathrm{e}^{-im\boldsymbol{v}\cdot\boldsymbol{\xi}/\hat{\hbar}_{\mathrm{c}}}\\ &\times\left\langle\Psi^\dagger\left(\boldsymbol{x}-\frac{\boldsymbol{\xi}}{2}\right)\Psi\left(\boldsymbol{x}+\frac{\boldsymbol{\xi}}{2}\right)\right\rangle, \end{aligned} \tag{8}$$

where $\Psi(\boldsymbol{x})$ is the quantum field operator, and $\langle\cdots\rangle$ stands for ensemble average. Eq.(8) is referred to as the Wigner quasi-distribution function, which can only

be interpreted as a probability distribution in the classical limit. Nevertheless, the macroscopic properties of the Wigner function are identical to the classical distribution, for example,

$$\int f(\boldsymbol{x},\boldsymbol{v})\mathrm{d}v = \left\langle \Psi^{\dagger}(\boldsymbol{x})\,\Psi(\boldsymbol{x})\right\rangle = \langle n(\boldsymbol{x})\rangle \tag{9}$$

is the average number density of the system. The dynamic behavior of the Wigner function is governed by the Wigner equation

$$\begin{aligned}(\partial_t + \boldsymbol{v}\cdot\partial_{\boldsymbol{x}})\, f(\boldsymbol{x},\boldsymbol{v},t) = \frac{1}{i\hat{\hbar}_{\mathrm{c}}}\int \mathrm{d}\boldsymbol{\xi}\int \frac{\mathrm{d}\boldsymbol{v}'}{(2\pi)^3} \\ \times \mathrm{e}^{i\left(\boldsymbol{v}'-\boldsymbol{v}\right)\cdot\boldsymbol{\xi}/\hat{\hbar}_{\mathrm{c}}}\left[\phi_+ - \phi_-\right] f(\boldsymbol{x},\boldsymbol{v}',t)\end{aligned} \tag{10}$$

in the collisionless limit. Here, $\phi_{\pm}$ is the abbreviation for $\phi(\boldsymbol{x}\pm\boldsymbol{\xi}/2)$. Along with the Poisson equation

$$-\nabla^2\phi = 4\pi e\left[Zn_i - \int \mathrm{d}\boldsymbol{v} f(v)\right], \tag{11}$$

where Z is the charge number of ions, the system is closed. The term "collisionless" in QKT is equivalent to the term "Hartree mean-field approximation" in DFT based methods [15].

Noticing that if the time, coordinate, and velocity variables in the above expressions are normalized to the inverse of plasma frequency ω_{p}^{-1}, the Thomas-Fermi screen length $\lambda_{\mathrm{F}} = v_{\mathrm{F}}/\omega_{\mathrm{p}}$ and the Fermi velocity $v_{\mathrm{F}} = \sqrt{2\mathcal{E}_{\mathrm{F}}/m_e}$, respectively, we shall replace the general NPC $\hat{\hbar}_{\mathrm{c}}$ by $\hat{\hbar}_{\mathrm{F}}$.

B. Numerical Method

The cumbersome phase-space integration in the Wigner equation makes the numerical solving not as straightforward as the Vlasov equation. The first numerical approach for Wigner equation was proposed by Suh in Ref. [24]. This approach is based on the splitting method [25], which was widely used and proven to be quite robust in solving the Vlasov equation, where the partial derivatives on the coordinate and velocity directions are treated separately. As velocity integral of Wigner equation can only be efficiently solved by Fourier spectrum method (FSM), Suh's method [24] uses FSM to advance both the coordinate and velocity direction. However, our benchmark simulations indicate that the long-time results of Suh's method are unsatisfactorily "noisy". Although there might exist some room for further improvement under Suh's pure FSM framework, we here invent or adopt a new numerical method: the flux balance method (FBM) [26] is used to advance the coordinate direction and FSM is used to the velocity direction. In order to distinguish Suh's pure FSM method, our method is here referred as hybrid splitting method (HSM). Benchmark simulations show that, in the case of long-time nonlinear simulations, our method, although simple, could ensure the smoothness of phase space and energy conservation. A detail comparison between Suh' method and our HSM method is displayed in Fig. 2.

III. PLASMON DECAY AND QUANTUM LANDAU DAMPING

The direct linearization of Eq.(10) yields the famous random phase approximation (RPA) [27]:

$$\epsilon(\omega,\boldsymbol{k}) = 1 + \frac{4\pi e^2}{k^2}\Pi_0(\omega,\boldsymbol{k}) = 0, \tag{12}$$

where

$$\Pi_0(\omega,\boldsymbol{k}) = \int \mathrm{d}\boldsymbol{p}\frac{f(\boldsymbol{p}) - f(\boldsymbol{p}+\hbar\boldsymbol{k})}{\hbar\omega - \boldsymbol{k}\cdot\hbar\boldsymbol{v} - \hbar^2k^2/2m} \tag{13}$$

is the Lindhard response function [28]. In the classical limit, where the wave length of collective mode is much longer than the wave length of electron, i.e., $|\boldsymbol{k}| \ll |\boldsymbol{p}|/\hbar$, Eq.(12) becomes

$$\epsilon(\omega,\boldsymbol{k}) = 1 - \frac{4\pi e^2}{k^2}\int \mathrm{d}\boldsymbol{p}\frac{\boldsymbol{k}\cdot\partial_{\boldsymbol{p}} f(\boldsymbol{p})}{\omega - \boldsymbol{k}\cdot\boldsymbol{v}}, \tag{14}$$

which is the well-know dielectric function of classical plasma. By assuming small damping rate, the real part and the imaginary part of the Lindhard function (13) are calculated separately:

$$\begin{aligned}\mathrm{Re}[\Pi_0] = \frac{\pi}{\mathcal{E}_{\mathrm{F}}\hat{k}}\mathcal{P}\int_0^{\infty}\mathrm{d}\hat{p}\,\hat{p} f(\hat{p}) \\ \times\left[\ln\left(\frac{\hat{p}-A_+}{\hat{p}+A_+}\right) - \ln\left(\frac{\hat{p}-A_-}{\hat{p}+A_-}\right)\right],\end{aligned} \tag{15}$$

$$\mathrm{Im}[\Pi_0] = \frac{3\pi^2 n}{8\mathcal{E}_{\mathrm{F}}k}\ln\frac{1+\exp\left[\left(A_+^2-\hat{\mu}\right)/\Theta\right]}{1+\exp\left[\left(A_-^2-\hat{\mu}\right)/\Theta\right]}, \tag{16}$$

where

$$A_{\pm} \equiv \hat{\hbar}_{\mathrm{F}}\frac{\hat{\omega}}{\hat{k}} \pm \frac{\hat{k}}{2}. \tag{17}$$

and $\hat{p} = p/p_{\mathrm{F}}$, $\hat{\omega} = \omega/\omega_{\mathrm{p}}$, $\hat{k} = k/k_{\mathrm{F}}$ are normalized quantities. As $\Theta \to 0$, an analytical result is obtained [28], i.e.,

$$\begin{aligned}\mathrm{Re}[\Pi_0] = \frac{3n}{4\mathcal{E}_{\mathrm{F}}}\left[1 + \frac{k_{\mathrm{F}}}{2k}\left(1-A_-^2\right)\ln\left|\frac{1+A_-}{1-A_-}\right|\right. \\ \left. -\frac{k_{\mathrm{F}}}{2k}\left(1-A_+^2\right)\ln\left|\frac{1+A_+}{1-A_+}\right|\right].\end{aligned} \tag{18}$$

It is clear from Eq.(15) that, when $|A_{\pm}| < 1$, Π_0 has no imaginary part. Thus, Eq.(12) is solved via the substitution of Eq.(18), and we plot the result in Fig. 3. The

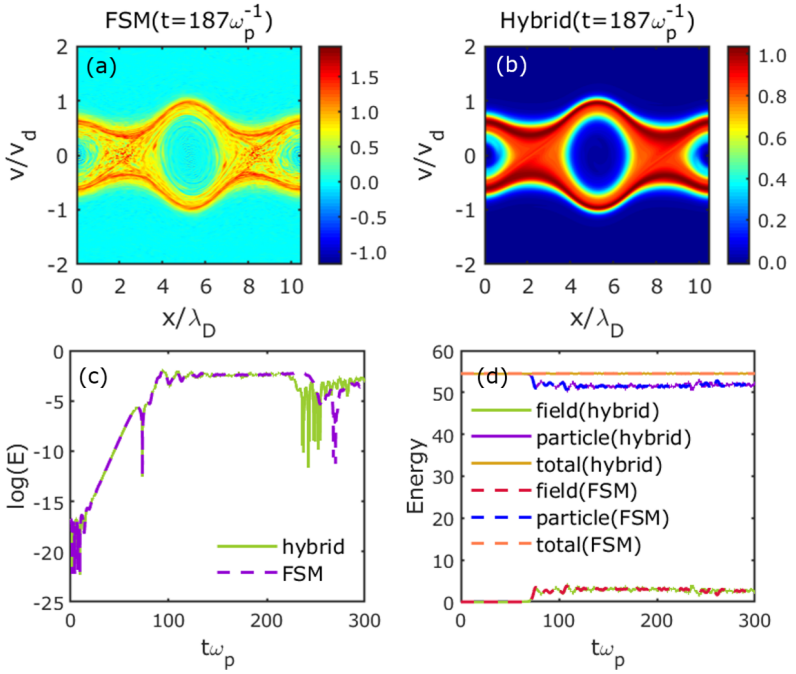

Figure 2. Comparison between pure FSM and HSM. (a) and (b) plotted the phase space snapshot of a classical BGK hole calculated by FSM and HSM respectively. (c) and (d) plotted the electric field and energy of each component of the system calculated by the two methods.

dashed-line stands for a false solution from the small damping approximation. At zero temperature, there is still an electron-hole excitation continuum (the area where $|A_{\pm}| > 1$) in which the cold plasmons are absorbed by the electrons, although there is no Landau damping [29]. This phenomenon can be demonstrated by our linear simulation. Note, we always keep $\hat{\hbar}_{\mathrm{F}} = 1$ in this section for convenience, which corresponds to a plasma with number density $n = 1.74 \times 10^{22}\mathrm{cm}^{-3}$.

A linear simulation result is plotted in Fig. 3, where the frequency of plasmons is represented by red crosses and the damping rate $(-\gamma/\omega_{\mathrm{p}})$ by inverted triangles. One can see that the plasmons with finite damping rate are those that fall within the plasmon decay continuum, while those fall outside the continuum are almost identical to the Lindhard solution. From Eq.(13), we find that a plasmon when satisfying the Cerenkov condition:

$$\omega - kv - \frac{\hbar k^2}{2m} = 0, \tag{19}$$

yields a pole of the integration, which is analog to the wave-particle resonant condition $\omega - kv = 0$ in classical plasmas. The wave-particle interaction in quantum plasmas is essentially a wave-wave interaction. Defining $q = mv/\hbar$ and $E_{\boldsymbol{q}} = \hbar^2 q^2/2m$, then Eq.(19) become

$$\hbar\omega = \frac{\hbar^2 (k+q)^2}{2m} - \frac{\hbar^2 q^2}{2m} = E_{\boldsymbol{k}+\boldsymbol{q}} - E_{\boldsymbol{q}}. \tag{20}$$

The physical intension is rather clear: a plasmon with energy $\hbar\omega$ is absorbed by an electron with energy $E_{\boldsymbol{q}}$. Fig. 4(a) plotted the Cerenkov match condition of a plasmon with $(\omega/\omega_{\mathrm{p}}, k/k_{\mathrm{F}}) = (1.58, 1.05)$. This plasmon is absorbed by an electron slightly below the Fermi surface, and kicks the electron out of the Fermi sea. Noticing that the electron obeys the dispersion relation

$$\omega = \frac{\hbar k^2}{2m}. \tag{21}$$

Actually, from Fig. 4(b), we can see that there are indeed a bunch of electrons excited to the corresponding location. However, such a high-energy electron beam may not always be observed, especially in higher wave number cases, due to nonlinear phase mixing or quantum correlation.

As the temperature rises, the role of the thermal Landau damping begins to emerge. In order to obtain the exact solution of Eq.(12), we need to extend the domain of definition of ω to the region where $\mathrm{Im}[\omega] < 0$ by means of analytic continuation, i.e.,

$$\Pi_0(\omega, \boldsymbol{k}) = \begin{cases} \int \mathrm{d}v_{\parallel} \dfrac{f^{-}_{\mathrm{FD1}} - f^{+}_{\mathrm{FD1}}}{\hbar\omega - k\hbar v_{\parallel}}, & \mathrm{Im}[\omega] > 0, \\ \int \mathrm{d}v_{\parallel} \dfrac{f^{-}_{\mathrm{FD1}} - f^{+}_{\mathrm{FD1}}}{\hbar\omega - k\hbar v_{\parallel}} & \\ \quad + \dfrac{2\pi i}{\hbar k} \left[f^{-}_{\mathrm{FD1}} - f^{+}_{\mathrm{FD1}} \right]_{v_{\parallel} = \frac{\omega}{k}}, & \mathrm{Im}[\omega] < 0, \end{cases} \tag{22}$$

where $f^{\pm}_{1\mathrm{FD1}} = f^{\pm}_{1\mathrm{FD1}}\left(p_{\parallel} \pm \hbar k/2\right)$, and the extra term in $\mathrm{Im}[\omega] < 0$ region comes from the residue of the integrand at the pole $v_{\parallel} = \omega/k$. In Fig. 5, we calculated $\Theta = 0.2,\ 1$

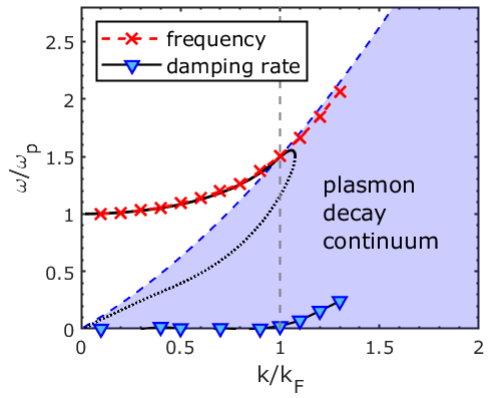

Figure 3. Numerical result of zero-temperature ($\Theta = 0.01$) plasmon decay. The black solid line and dotted line is calculated from Eq.(18).

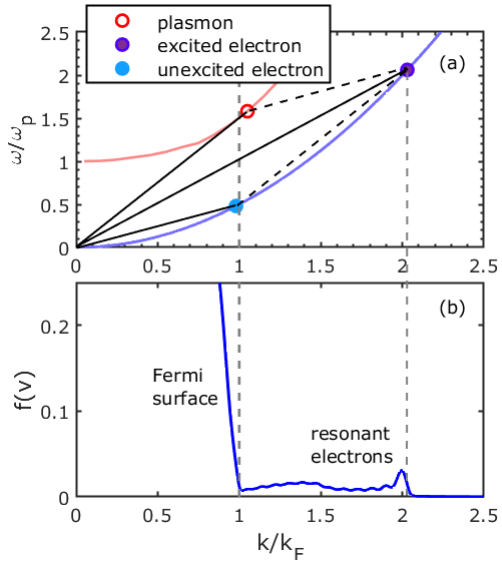

Figure 4. This figure presents the result of plasmon decay at $k = 1.05k_F$. (a) Cerenkov parallelogram matching condition. (b) Distribution function of electrons, where a small bunch of electrons are excited by plasmons.

and 2, which corresponding to $T = 5672$K, 28360K and 56720K, respectively, in a $\hat{\hbar}_F = 1$ plasma. These parameters roughly fall within the parameter range of WDM experiments [2, 6]. Similar results were obtained by Ref. [30], in which the authors adopted a PIC semi-classical simulation and did not include the quantum recoil effect.

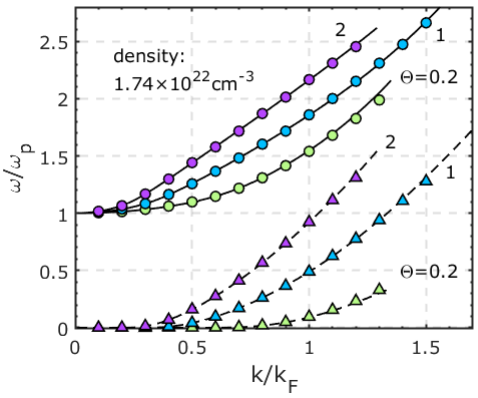

Figure 5. Linear Landau damping of a dense ($\hat{\hbar}_F = 1$) plasma. The solid lines and the dashed-lines are the real part and minus of imaginary part of the exact solutions of Eq.(12), while the circles and the triangles are the corresponding simulation results.

IV. QUANTUM TWO-STREAM INSTABILITY AND THE QUANTUM BGK MODE

A. Linear Result

Two-stream instability in quantum plasmas has been investigated by many authors [31–35]. However, despite the fact that two-stream instability is a reactive-type instability, namely the instability driven by the Hermitian part of the dielectric function [36], the real world plasma always possess finite temperature. Especially in a high-density plasma, the Pauli exclusive principle ensures the electrons have finite velocities even at zero temperature. Thus, regardless of the reliability of QHD, a kinetic method is needed, as is pointed out in Ref. [31] and Ref. [34].

In the fluid limit, it is convenient to define another NPC:

$$\hat{\hbar}_d = \hbar\omega_p/mv_d^2, \tag{23}$$

where v_d is the relative drift velocity of the two streams. Hence the eigen-mode frequency of quantum fluid two-stream instability can be written as [34, 37]

$$\omega = \frac{\omega_p}{\sqrt{2}}\Big[1 + 2\hat{\hbar}_d\tilde{k}^2 + \frac{\hat{\hbar}_d^2\tilde{k}^4}{2} \pm\sqrt{1 + 8\tilde{k}^2 + 4\hat{\hbar}_d^2\tilde{k}^6}\Big]^{\frac{1}{2}}, \tag{24}$$

where $\tilde{k} = kv_d/\omega_p$. As is shown in the left panel of Fig. 6, the quantum recoil effect creates an extra unstable region which hides itself at $k = \infty$ when $\hat{\hbar}_d = 0$. As $\hat{\hbar}_d$ increases, this unstable quantum "bubble" moves toward longer wavelength and absorbed by the original unstable bubble at a certain value of $\hat{\hbar}_d$. Noticing that the quantum bubble is always located in relatively high

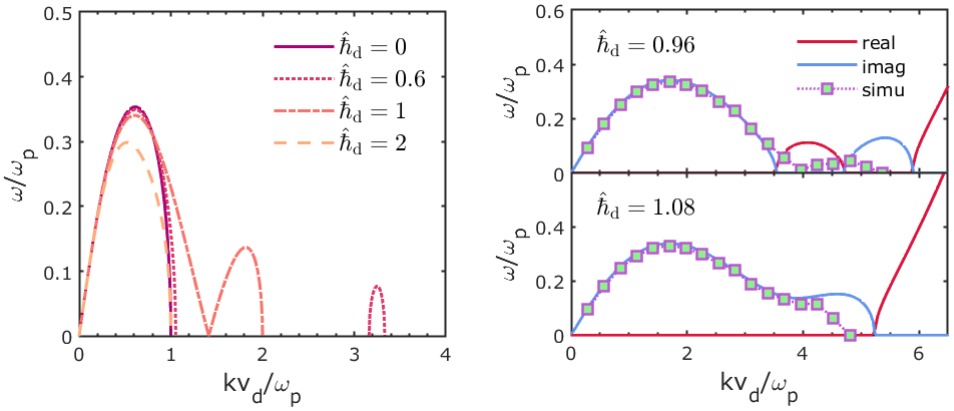

Figure 6. Dispersion relation of quantum two-stream instability varying with $\hat{\hbar}_d$ (left). Simulation of the extra unstable region created by quantum recoil effect (right).

wave-number region, where any disturbance is heavily Landau damped. As a result, this unstable region may not exist in real dense plasma. In the right panel of Fig. 6, we simulated a quantum two-stream instability around $\hat{\hbar}_d = 1$ with an exaggerated drift velocity, i.e., $v_d = 50v_F$, in order to eliminate the kinetic effect. Even so, the numerical approach still can not reproduce the quantum bubble calculated by Eq.(24), except for some distortion in the high wave number region.

We will show that the quantum effect has the most impact in the nonlinear phase in the next sections by consider a more realistic quantum plasma with a reasonable ratio of Fermi velocity to drift velocity.

B. BGK Equilibrium in Partial Quantum System

It is shown by Bernstein, Green and Kruskal [38] that there exists a nonlinear equilibrium mode, namely, the BGK mode, in an electron electrostatic plasma. The BGK mode is ubiquitous in the field of plasma physics because it provides a important kinetic nonlinear saturation mechanism for many plasma instabilities. The onset of particle trapping in quantum Landau damping is briefly discussed in Ref. [30], where the potential trough that traps the particle is rather shallow because this trapping process occurs after a period of Landau damping. Here, we set up a BGK equilibrium by a symmetrical electron two-stream system to investigate the particle trapping process in quantum plasma. To see how quantum recoil effect affects the BGK mode, we scan the NPC $\hat{\hbar}_T$ from 0 (Vlasov equation) to 10. As $\hat{\hbar}_T$ increases, which means that the temperature decreases and the density increases, quantum recoil effect will eventually become dominant and the kinetic effect disappears. A system in the state in which kinetic effects completely disappear is referred to as a fully quantum system, and the medium state between quantum and classical systems is called partial quantum system.

The snapshots of typical moments of the development of a classical BGK mode are presented in the upper panels of Fig. 7. The panel (a) stands for the end of linear growth, and the electron beams start to twist. In panel (b), electrons with velocity near the wave velocity (which is equal to zero in our wave frame of reference) bounce off the potential barrier and complete a full cycle at panel (c). A nearly steady state is formed after several bounce period, as is shown in panel (d).

In lower panel of Fig. 7, where $\hat{\hbar}_T = 0.8$, one can see that, from panel (e) to (h), the basic shape of a classical BGK hole is preserved. This is a typical partial quantum system. Consider a pure state harmonic oscillator, the Wigner representation of which is [39]

$$w_n(x,p) = \frac{1}{\pi}\left(\frac{1}{4}\right)^n e^{-(x^2+p^2)} \times \sum_{k=0}^{n} \frac{H_{2k}\left(\sqrt{2}x\right) H_{2(n-k)}\left(\sqrt{2}p\right)}{k!(n-k)!}, \tag{25}$$

where H_n is the n-th order Hermitian function, and thus n is the quantum number of a quantum harmonic oscillator. The pictorial representation of Eq.(25) is a ripple-like structure, which is exactly like what we have found in the nonlinear saturation phase of the $\hat{\hbar}_T = 0.8$ quantum BGK mode, as is shown in Fig. 7(d). The physical interpretation is rather clear: the hollow structure in classical BGK mode is nothing but the phase space representation of a classical oscillator, hence it is not surprising to find a quantum oscillator in a quantum BGK mode.

C. Periodic Solution in Full Quantum System

We examine a full quantum system further by increasing the product of the NPC $\hat{\hbar}_F$ and wave number $\hat{k}$, which indicates the ratio of energy and momentum between a plasmon and an electron sitting on the Fermi surface.

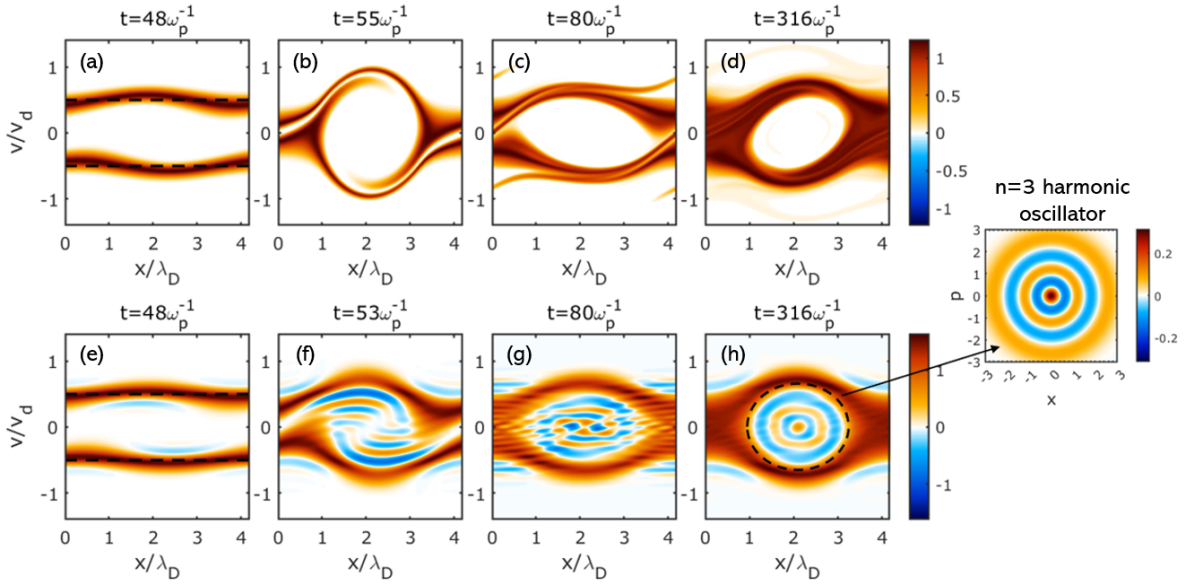

Figure 7. (a) to (d): BGK equilibrium in classical plasma. (e) to (h) BGK equilibrium in partial quantum plasma, a $n = 3$ quantum oscillator is formed at the nonlinear stage.

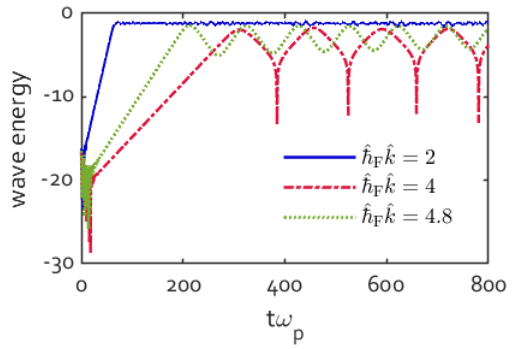

Figure 8. Energy evolution of two-stream instability with different values of $\hat{\hbar}_F\hat{k}$.

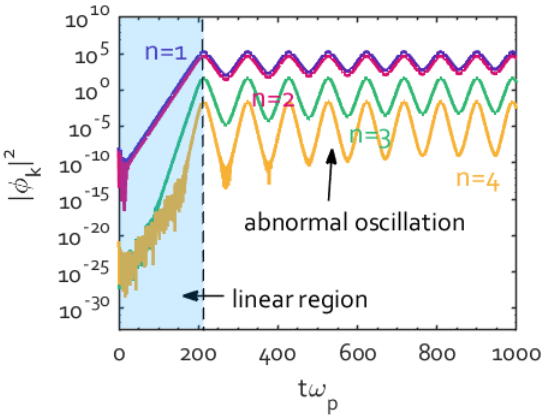

Figure 9. Abnormal oscillation of a $\hat{\hbar}_F\hat{k} = 4.8$ quantum two-stream instability, the harmonics grow and damp with its corresponding linear growth rate.

The energy of the resonant mode of three typical parameters is presented in Fig. 8, from which we found that when $\hat{\hbar}_F\hat{k} = 2$ the wave energy is almost constant in the nonlinear saturation phase, and this is corresponding to the quantum BGK equilibrium we have discussed in the previous section. When the value of $\hat{\hbar}_F\hat{k}$ is high enough, one can see that an interesting phenomenon occurs at the nonlinear phase: when the electric potential reach its linear limitation, instead of saturating into a relatively steady state, the wave damps to equilibrium level with the damp rate exactly equal to the opposite of the linear growth rate, and then growing back to linear limitation, and so on and so forth. This nearly periodic anomalous oscillation does not fade away after hundreds of plasma oscillation periods if there is no dissipation mechanism. The evolution of the harmonics of the $\hat{\hbar}_F\hat{k} = 4.8$ electric potential is plotted in Fig. 9. Noticing that this intriguing phenomenon is quite analog with what is reported in Ref. [37] by means of quantum Dawson model, i.e., a coupled Schrödinger-Poisson model. The quantum Dawson model is approximately equivalent to the Wigner-Poisson model, when the number of pure states N is large enough.

The abnormal oscillation is result from the energy exchange between electrons and the plasmon. The momentum of the plasmon, i.e., the wave number of the quantum Langmuir wave, must obeys the condition

$$\hat{\hbar}_F\hat{k} \gtrsim \hat{v}_d - 2, \tag{26}$$

or, equivalently,

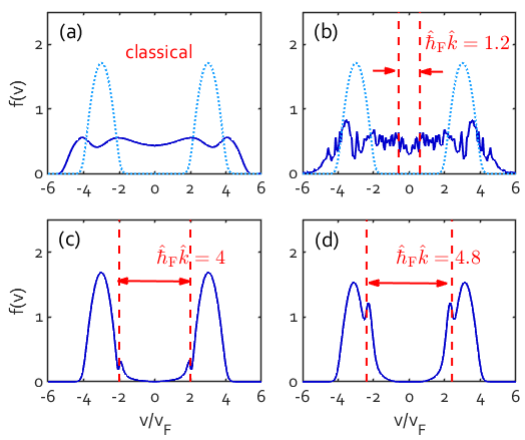

Figure 10. Velocity distribution of (a) classical BGK equilibrium, (b) quantum BGK equilibrium, (c)(d) the peak of the abnormal oscillation. The dotted-line stands for the initial distribution.

$$\frac{\hbar k}{m} \gtrsim \frac{1}{2}\left(v_{\mathrm{d}} - 2v_{\mathrm{F}}\right). \tag{27}$$

This condition is not exact because there are always thermal electrons outside of the Fermi surface when the temperature is finite. As shown in Fig. 10, the drift velocity of the two electron beams is $6v_{\mathrm{F}}$, thus the normalized momentum of a plasmon $\hat{\hbar}_{\mathrm{F}}\hat{k}$ should be approximately larger than 4. Panel (a) is a classical BGK equilibrium, while panel (b) is a quantum BGK equilibrium where the wave-length of the resonant mode does not satisfy the threshold condition (26), hence there the abnormal oscillation does not occur. On the contrary, in panel (c) and (d), while the velocity distribution at the peak of the abnormal oscillation is plotted, we find that a pair of electron bunch is excited according to the Cerenkov condition (19). Thus, this abnormal oscillation stems from the wave-wave energy exchange, which is the quantum version of the wave-particle energy exchange mechanism in classical plasma physics.

V. CONCLUSION AND DISCUSSION

In this paper, the Wigner-Poisson system is numerically solved by using a hybrid numerical scheme in order to investigate the quantum nature of dense plasmas. Our hybrid numerical scheme, although is simple, shows significant advantages in energy conservation and smoothness of phase space. The linear results of simulations are benchmarked with RPA theory. The thermal effect to linear quantum Landau damping is also benchmarked by both eigenvalue method and time-dependent initial value method, which show almost identical results.

In the nonlinear region, the role of quantum recoil effect in dense plasma is studied in detail. The BGK equilibrium formed by two counter-flowing electron beams demonstrates an interesting yet perspicuous quantum mechanical phenomenon. When the wavelength of wave function of electron is much shorter than the wavelength of the collective mode but still long enough such that the wave effect cannot be ignored, the electrons trapped in the potential trough form a quantum oscillator in phase space. When the scale of the two wave-length is comparable and a threshold condition is satisfied, the energy exchange between the electron and collective mode result in an abnormal oscillation which does not exist in classical plasmas.

ACKNOWLEDGMENTS

This work was supported by National Natural Science Foundation of China 11875235, 61627901, 12075204), the Strategic Priority Research Program of Chinese Academy of Sciences (Grant No. XDA250050500).

[1] G. Manfredi. How to model quantum plasmas. *Fields Institute Communications*, 46:263–287, 2005.
[2] S. H. Glenzer, O. L. Landen, P. Neumayer, RW Lee, K. Widmann, S. W. Pollaine, R. J. Wallace, G. Gregori, A. Höll, Th Bornath, et al. Observations of plasmons in warm dense matter. *Physical Review Letters*, 98(6):065002, 2007.
[3] P. K. Shukla and Lennart Stenflo. Stimulated scattering instabilities of electromagnetic waves in an ultracold quantum plasma. *Physics of plasmas*, 13(4):044505, 2006.
[4] A. C. Hayes, M. E. Gooden, E. Henry, Gerard Jungman, J. B. Wilhelmy, R. S. Rundberg, C. Yeamans, G. Kyrala, C. Cerjan, D. L. Danielson, et al. Plasma stopping-power measurements reveal transition from non-degenerate to degenerate plasmas. *Nature Physics*, 16(4):432–437, 2020.
[5] J. Daligault and S. Gupta. Electron–ion scattering in dense multi-component plasmas: Application to the outer crust of an accreting neutron star. *The Astrophysical Journal*, 703(1):994, 2009.
[6] Tobias Dornheim, Simon Groth, and Michael Bonitz. The uniform electron gas at warm dense matter conditions. *Physics Reports*, 744:1–86, 2018.
[7] P. Hohenberg and W. Kohn. Inhomogeneous electron gas. *Physical Review*, 136(3B):B864, 1964.
[8] Walter Kohn and Lu Jeu Sham. Self-consistent equations including exchange and correlation effects. *Physical Review*, 140(4A):A1133, 1965.
[9] Chang Gao, Shen Zhang, Wei Kang, Cong Wang, Ping Zhang, and X. T. He. Validity boundary of orbital-free molecular dynamics method corresponding to thermal ionization of shell structure. *Physical Review B*,

94(20):205115, 2016.

[10] Shen Zhang, Hongwei Wang, Wei Kang, Ping Zhang, and XT He. Extended application of kohn-sham first-principles molecular dynamics method with plane wave approximation at high energy – from cold materials to hot dense plasmas. *Physics of Plasmas*, 23(4):042707, 2016.

[11] Shen Zhang, Shijun Zhao, Wei Kang, Ping Zhang, and Xian-Tu He. Link between k absorption edges and thermodynamic properties of warm dense plasmas established by an improved first-principles method. *Physical Review B*, 93(11):115114, 2016.

[12] E. Wigner. On the quantum correction for thermodynamic equilibrium. *Physical Review*, 40:749–759, Jun 1932.

[13] Leo P. Kadanoff. *Quantum statistical mechanics*. W. A. Benjamin, Inc, 1962.

[14] D. Kremp, Th Bornath, M. Bonitz, and M. Schlanges. Quantum kinetic theory of plasmas in strong laser fields. *Physical Review E*, 60(4):4725, 1999.

[15] Giovanni Manfredi, Paul-Antoine Hervieux, and Jérôme Hurst. Phase-space modeling of solid-state plasmas. *Reviews of Modern Plasma Physics*, 3(1):1–55, 2019.

[16] Jiong-Hang Liang, Tian-Xing Hu, D. Wu, and Zheng-Mao Sheng. Kinetic studies of exchange-correlation effect on the collective excitations of warm dense plasmas. *Phys. Rev. E*, 105:045206, Apr 2022.

[17] G. Manfredi and F. Haas. Self-consistent fluid model for a quantum electron gas. *Physical Review B*, 64(7):075316, 2001.

[18] L. G. Garcia, F. Haas, L. P. L. De Oliveira, and J. Goedert. Modified zakharov equations for plasmas with a quantum correction. *Physics of Plasmas*, 12(1):012302, 2005.

[19] P. K. Shukla and B. Eliasson. Formation and dynamics of dark solitons and vortices in quantum electron plasmas. *Physical Review Letters*, 96(24):245001, 2006.

[20] Dastgeer Shaikh and P. K. Shukla. Fluid turbulence in quantum plasmas. *Physical Review Letters*, 99(12):125002, 2007.

[21] Padma Kant Shukla and Bengt Eliasson. Novel attractive force between ions in quantum plasmas. *Physical Review Letters*, 108(16):165007, 2012.

[22] M. Bonitz, E. Pehlke, and T. Schoof. Attractive forces between ions in quantum plasmas: Failure of linearized quantum hydrodynamics. *Physical Review E*, 87(3):033105, 2013.

[23] Michael Bonitz, Zh A. Moldabekov, and T. S. Ramazanov. Quantum hydrodynamics for plasmas – quo vadis? *Physics of Plasmas*, 26(9):090601, 2019.

[24] Nam-Duk Suh, Marl R. Feix, and Pierre Bertrand. Numerical simulation of the quantum liouville-poisson system. *Journal of Computational Physics*, 94(2):403–418, 1991.

[25] Chio-Zong Cheng and Georg Knorr. The integration of the vlasov equation in configuration space. *Journal of Computational Physics*, 22(3):330–351, 1976.

[26] Francis Filbet, Eric Sonnendrücker, and Pierre Bertrand. Conservative numerical schemes for the vlasov equation. *Journal of Computational Physics*, 172(1):166–187, 2001.

[27] David Pines and David Bohm. A collective description of electron interactions: II. collective vs individual particle aspects of the interactions. *Physical Review*, 85(2):338, 1952.

[28] J. Lindhard. On the properties of a gas of charged particles. *Dan. Vid. Selsk Mat.-Fys. Medd.*, 28:8, 1954.

[29] V. S. Krivitskii and S. V. Vladimirov. The spectrum of electronic vibrations in a degenerate nonrelativistic plasma. *Soviet Journal of Experimental and Theoretical Physics*, 73(5):821, 1991.

[30] Jérôme Daligault. Landau damping and the onset of particle trapping in quantum plasmas. *Physics of Plasmas*, 21(4):040701, 2014.

[31] Seunghyeon Son. Two-stream instabilities in degenerate quantum plasmas. *Physics Letters A*, 378(34):2505–2508, 2014.

[32] Fernando Haas and Bengt Eliasson. A new two-stream instability mode in magnetized quantum plasma. *Physica Scripta*, 90(8):088005, 2015.

[33] A. Bret and F. Haas. Connection between the two branches of the quantum two-stream instability across the k space. *Physics of Plasmas*, 17(5):052101, 2010.

[34] Jiong-Hang Liang, Tian-Xing Hu, D. Wu, and Zheng-Mao Sheng. Kinetic study of quantum two-stream instability by wigner approach. *Physical Review E*, 103(3):033207, 2021.

[35] F. Haas, A. Bret, and P. K. Shukla. Physical interpretation of the quantum two-stream instability. *Physical Review E*, 80(6):066407, 2009.

[36] Liu Chen. *Waves and instabilities in plasmas*, volume 12. World scientific, 1987.

[37] F. Haas, G. Manfredi, and M. Feix. Multistream model for quantum plasmas. *Physical Review E*, 62(2):2763, 2000.

[38] Ira B. Bernstein, John M. Greene, and Martin D. Kruskal. Exact nonlinear plasma oscillations. *Physical Review*, 108(3):546, 1957.

[39] Young-Suk Kim and Marilyn E. Noz. *Phase space picture of quantum mechanics: group theoretical approach*, volume 40. World Scientific, 1991.